Substrate Dissipation Energy Regulates Cell Adhesion and Spreading

Pasquale Sacco, Gabriele Baj, Fioretta Asaro, Eleonora Marsich, and Ivan Donati*

Recent evidence has led to the hypothesis that dissipation of energy through the viscoelastic extracellular matrix (ECM) can play a cardinal role in directing cell-fate decisions, but whether and how it correlates with specific cell response is at present unclear. Here, viscoelastic and plastic 2D chitosan-based substrates endowed with different dissipative energies are developed and cell behavior studied in terms of adhesion and spreading. While keeping constant stress relaxation and systematically decoupling overall stiffness from linear elongation, an energy dissipation term (J mol^{-1}) is introduced, that is the molar energy required to deviate from linear stress–strain regime and enter into plastic region. Strikingly, an inverse relationship is unveiled between substrate dissipation energy and cell response, with high adhesion/high spreading and low adhesion/no spreading detected for substrates at low and high dissipation energy, respectively. It is concluded that cells decide how to react depending on the effective energy they can earmark for their functions.

1. Introduction

Over the last two decades mechanical cues have been identified as key regulators in directing cell-fate decisions, influencing behavior and differentiation, tissue development and regeneration or eliciting onset of various pathologies such as cancer and cardiovascular diseases.[1–6] In this scenario, cells perceive surrounding extracellular matrix (ECM) nature and respond accordingly. Hence, ECM substrate does not act as static and passive but as dynamic mechanotransducer in sparking intracellular biochemical pathways.[7] Enormous efforts have been therefore undertaken hitherto to understand this subtle substrate-to-cell relationship.

Purely 2D elastic materials have been massively employed as original model to investigate cell functions.[1,8–11] The mechanistic basis for triggering biological processes resides in the concept that cells pull on ECM network and gauge the feedback to make their fate decisions.[9] This vision supports the idea that substrate energy, depending in turn on inherent stiffness and whole linear elongation, is constantly stored over time, thus traction forces exerted by cells may be, in principle, totally converted into feedback reaction. Yet, most of ECMs composing native tissues are viscoelastic substrates in nature,[12–14] so that overall stresses are relaxed by viscous contributions or following to ECM yielding (plastic behavior); as a result, collected energy is progressively dissipated. This simple but effective evidence has paved the way to novel considerations on how cells probe and integrate substrate mechanics. Stress relaxation has been recently introduced as potent factor in instructing cells how to react,[14–18] therefore the "energy-dissipative" contribution cannot be neglected at all in cell mechanobiology. As proof of evidence, it has been recognized that substrate viscosity can compensate reduced elasticity in regulating cell response.[19] Given these premises, it results straightforward that the crosstalk between cells and ECM is energetic in origin, and recent findings seem confirming this vision,[11,20] but whether and how energy linked to substrate correlates with specific cell behavior remains elusive.

Here we address this open question by fabricating substrates at different dissipative energy and subsequently studying cell response in terms of adhesion and spreading. From the mere material point of view, we assembled joint viscoelastic and plastic chitosan-based gels, which represent inborn permissive cell-adherent 2D substrates.[21] Next, we systematically decoupled substrate stiffness—that envisages the stored purely elastic energy before material entering into plastic regime—from linear elongation while keeping constant stress relaxation by changing polymer chemical composition and type of cross-linker used to set up gels. Three energy dissipation ranges have been identified and correlated with cell response, highlighting the role played by substrate "energy dampers" as cardinal actors in making cell-fate decisions. Entailing Bernoullian and Markov chain zeroth-order statistics,[22] we finally identified substrate sugar sequences, i.e., the energy dampers, engaged in damping cell traction forces.

Dr. P. Sacco, Dr. G. Baj, Prof. I. Donati
Department of Life Sciences
University of Trieste
Via Licio Giorgieri 5, Trieste I-34127, Italy
E-mail: psacco@units.it
Dr. F. Asaro
Department of Chemical and Pharmaceutical Sciences
University of Trieste
Via Licio Giorgieri 1, Trieste I-34127, Italy
Dr. E. Marsich
Department of Medicine
Surgery and Health Sciences
University of Trieste
Piazza dell'Ospitale 1, Trieste I-34129, Italy

2. Results

2.1. Chitosan Chemical Composition Influences Substrate Viscoelasticity

At first, we synthesized a medium acetylated chitosan starting from a template showing fraction of acetylation, F_A, of 0.14. Taking advantage of a procedure entailing the use of a hydroalcoholic mixture and acetic anhydride as acetyl group donor,[23] we produced a chitosan sample with final F_A = 0.31 and an almost random distribution of the two building sugars, i.e., glucosamine (D unit) and *N*-acetyl-glucosamine (A unit), along polymer chain as shown by the similarity of dyad frequencies measured from ^{13}C-NMR analyses and theoretically calculated from Bernoullian statistical approach (Appendix 1, Supporting Information).[24]

With this two chitosans we produced ionically cross-linked gels as 2D cell substrates by exploiting the slow ion diffusion technique using tripolyphosphate (TPP) as gelling agent.[25] Resulting networks were plastic and viscoelastic as confirmed by the strain-softening behavior at large deformations, the frequency dependence of elastic modulus and the stress relaxation curve profiles over time (**Figure 1**a,c,e). Mathematical treatment of experimental data revealed straightforward differences

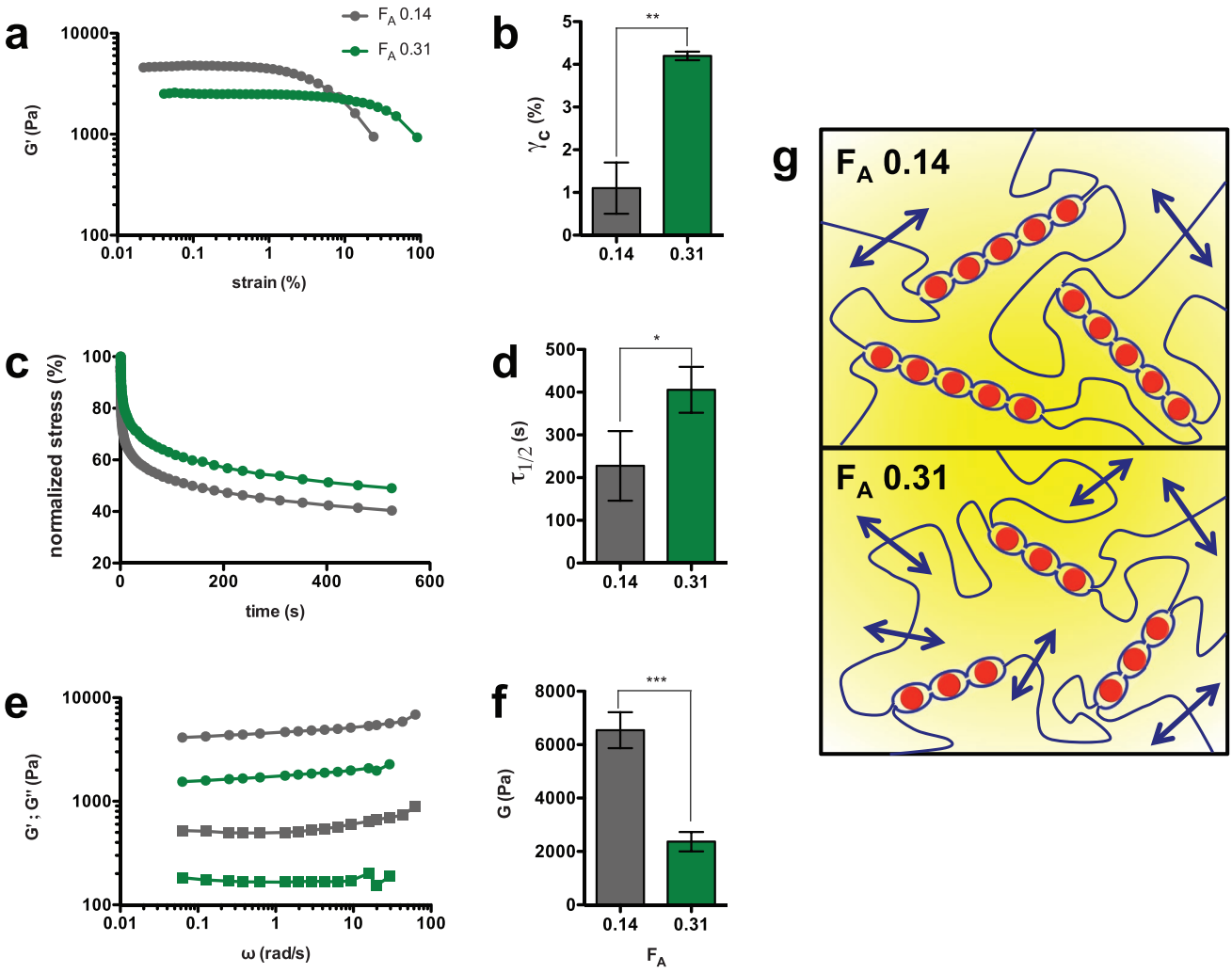

Figure 1. Chitosans at different chemical composition lead to the formation of cell substrates endowed with different mechanics. Ionically cross-linked gels based on chitosans at different fraction of acetylated units, F_A, were fabricated by means of the controlled TPP diffusion throughout chitosan solutions. a) Elastic modulus, G', profiles as a function of applied strain for gels at different chemical composition; strain sweep experiments were performed under a constant frequency of 1 Hz. b) Critical deformation, γ_c, at which strain-softening manifests for gels at different F_A; γ_c is determined according to the Soskey–Winter model (Appendix 2, Supporting Information). c) Curve profiles of normalized stress relaxation under a constant strain, γ= 1%, as a function of time for gels at different F_A. d) Time needed to relax the stress to half of the initial value, $\tau_{0.5}$, for gels at different F_A. e) Dependence of elastic, G', and viscous, G'', moduli as a function of angular frequency, ω, for gels at different F_A; mechanical spectra were recorded under a constant stress of 5 Pa. f) Shear moduli for gels at different chemical composition calculated by Maxwell model (Appendix 2, Supporting Information). All chitosan gels were fabricated with molar ratio between TPP and repeating unit of chitosan, r = [TPP]/[chitosan]$_{r.u.}$, equal to 5.2. Data are reported as mean ± s.d., n = 3–4 gels analyzed for each experimental condition. Statistics: *, $P < 0.05$; **, $P < 0.01$; ***, $P < 0.001$ (Student's t-test). g) Sketchy representation of chitosan-TPP junctions within gels at different chemical composition: in the case of F_A = 0.14, longer glucosamine sequences ensure higher gel stiffness with respect to F_A = 0.31 samples; on the opposite, shorter D-blocks, and ensuing A-blocks increment, endow gels with lower stiffness but higher stretching.

between the two systems in terms of mechanical performance, highlighting a diverse extent of linear elongation, with critical deformation marking onset of strain-softening, γ_c, greater for F_A = 0.31 chitosan gels than lower acetylated counterparts (Figure 1b), in nice agreement with our previous results.[26] The time needed to relax the stress to half of the initial value, $\tau_{0.5}$, is in line with timescales detected for analogous ionic gelling systems (Figure 1d).[14,27] Calculation of gel stiffness (Appendix 2, Supporting Information) yielded shear moduli of 6.5 ± 0.7 and 2.4 ± 0.4 kPa for gel composed of F_A = 0.14 and 0.31 chitosans, respectively (Figure 1f). Taken together, this set of findings demonstrates the inverse relationship between gel stiffness and linear elongation: low acetylated chitosan sample allowed for the formation of more rigid and less stretchable networks, whereas medium acetylated counterpart assembled weaker and more stretchy gels (Videos S1 and S2, Supporting Information). The different mechanical nature resides in the fraction and statistical sequence of monomers along polymer chain, exhibiting average block D length, N_D, of 5.1 and 2.9 for gel composed of F_A = 0.14 and 0.31 chitosans, respectively (Table S1, Supporting Information). Hence, longer adjacent glucosamine units adequate for TPP ionic binding endow chitosan-based gels with higher rigidity, whereas greater amounts of A-type blocks are associated with the extension of linear region toward large deformations (Figure 1g).

2.2. Decoupling Viscoelastic Contributions to Correlate Substrate Mechanics with Cell-Fate Decisions

With these substrates we next studied the effect of gel mechanics on cell adhesion and spreading. We systematically decoupled viscoelastic contributions by adjusting the amount or changing the type of cross-linker to assemble gels. In the first case, the concentration of TPP was reduced to produce a set of substrates showing similar stress relaxation but different stiffness and critical elongation (**Figure 2**a–c). When mouse fibroblasts NIH-3T3 were incubated with gels at different F_A we observed differences in terms of adherent cells (Figure 2d,e), as proved by the notable reduction of the fluorescence signal as well as total cell number/substrate area detected for F_A = 0.31 chitosan gels with respect to lower acetylated substrates. Furthermore, cell spreading was affected by gel mechanics: while NIH-3T3 nicely spread atop substrates exhibiting higher stiffness and lower elongation (F_A = 0.14 chitosan gels) as confirmed by well-polymerized F-actin filaments and overall cell spreading area (Figure 2f,g), F_A = 0.31 chitosan gels did not promote any cell spreading (Figure 2f,h). This condition was accompanied with higher cell death noticed for F_A = 0.31 substrates as indicated by larger levels—at the relative scale—of LDH enzyme released by cells into the incubation medium (Figure S7, Supporting Information).

We next fabricated chitosan gels with same chemical composition (F_A = 0.14 chitosan) but different cross-linker to produce a set of substrates matching stress relaxation and critical elongation but showing different stiffness (Figure 2i–k). Pyrophosphate (PPi) was selected as alternative gelling agent to reticulate chitosan due to its ability to form tridimensional gels as TPP but with lower stiffness.[28] With this new set of substrates, we observed comparable number of adherent NIH-3T3 atop chitosan gels reticulated by either TPP or PPi (Figure 2l,m), but different rate of cell spreading (Figure 2n–p). Even in the case of PPi-based substrates, shortage of cell spreading correlated with larger cell death (Figure S7, Supporting Information).

To get insights on how substrate mechanics linked to cell-fate decisions, human osteosarcoma MG-63 were incubated atop permissive F_A = 0.14 chitosan-TPP substrates in the presence or absence of the β-1 integrin blocking antibody (**Figure 3**a). Furthermore, NIH-3T3 were incubated with different cytoskeleton polymerization inhibitors and the total amount of adherent cells quantified colorimetrically (Figure 3b). Specifically, cells were incubated with the following chemicals: blebbistatin (inhibitor of myosinII ATP-ase), ML-7 (inhibitor of myosin light chain kinase), Y-27632 (inhibitor of Rho-associated kinase), and cytochalasin D (inhibitor of actin polymerization).[10,15] Collectively, this set of experiments provided evidence that β-1 integrin was involved in cell adhesion mechanism,[29] whereas cytoskeleton polymerization machinery was not, suggesting that cell adhesion and spreading were temporally coordinated.[30] This statement was indirectly confirmed by the fact that the overall spreading was hampered for well-adherent cells in the presence of cytochalasin D (Figure 3c). Of note, cell spreading was accompanied with nuclear translocation of transcriptional regulator Yes-associated protein (YAP) (Figure 3d), as well as formation of β-1 integrin-based punctual focal adhesions (Figure 3e), clearly indicating that F_A = 0.14 chitosan-TPP gels behaved as mechanotransducer substrates.[31,32]

2.3. Substrates at Different Dissipation Energy Regulate Cell Response

While keeping constant stress relaxation, substrate stiffness and critical elongation together represent, in principle, the main contributions that governed cell adhesion and spreading atop 2D chitosan-based gels. Here, we raise the possibility to merge these two effects into a singular parameter for investigating, and eventually predicting, cell behavior on substrates at different mechanics. From the combined analysis of frequency and strain sweep data we calculated the molar energy (J mol^{-1}) required to deviate from linear stress–strain regime (Appendix 2, Supporting Information), that describes the work generated by shear forces before material starting to irreversibly deform, i.e., entering into plastic region (**Figure 4**a).[26] With this approach we identified three different energy (E_d) regimes (Figure 4b), which can be correlated with our biological findings:

i. regime I, E_d = 0.19 ± 0.09 J mol^{-1}, high cell adhesion and high spreading;
ii. regime II, E_d = 0.42 ± 0.29 J mol^{-1}, high cell adhesion but low spreading;
iii. regime III, E_d = 1.58 ± 0.47 J mol^{-1}, low cell adhesion and no spreading.

Since the magnitude of work generated by shear forces in the linear stress–strain region markedly depended on energy dissipation phenomena due to chitosan chemical composition,[26] we here define E_d as an energy dissipation term. As

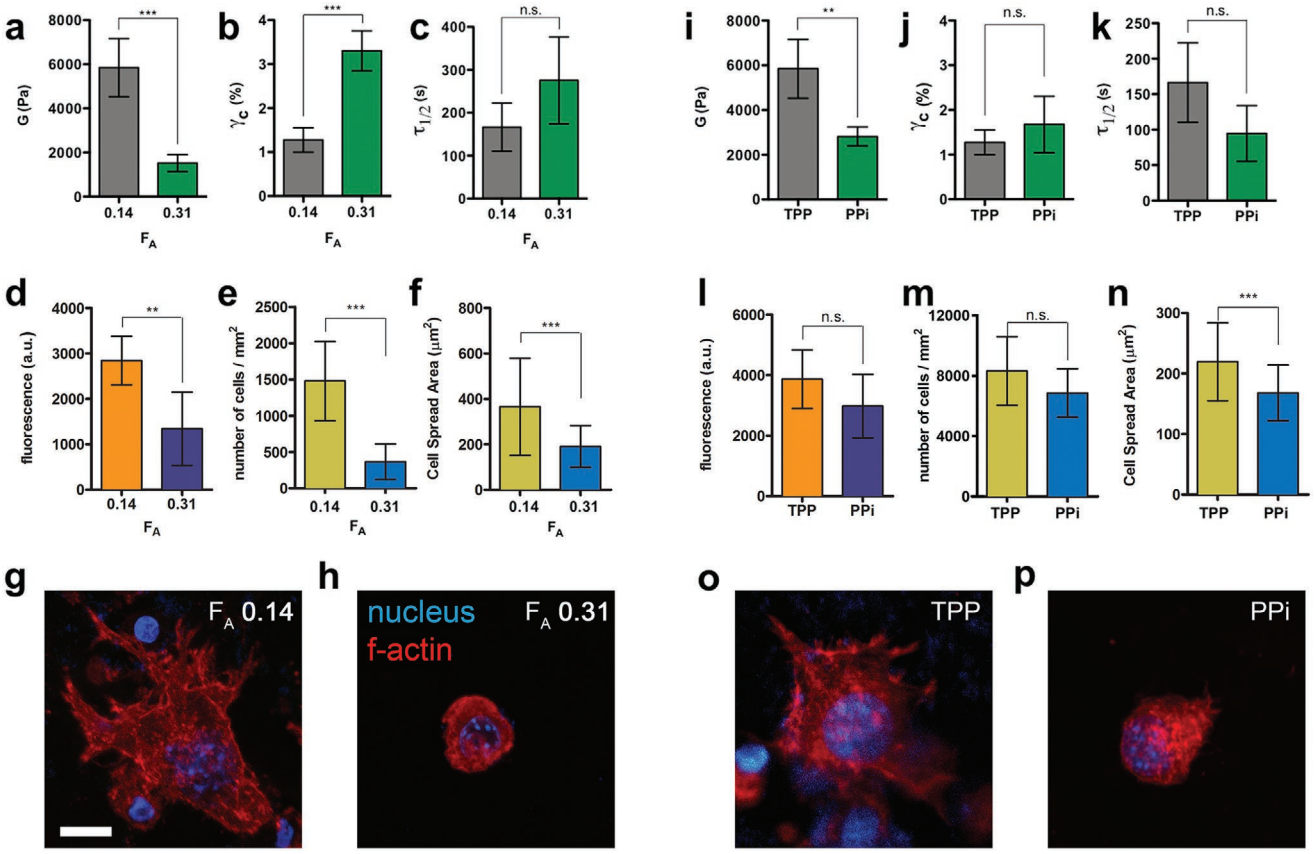

Figure 2. Cell adhesion and spreading are modulated by systematically tuning overall substrate elongation and stiffness while keeping constant stress relaxation. a–c) Shear modulus, critical elongation, and stress relaxation for ionically cross-linked gels based on chitosans at different chemical composition but same cross-linker, i.e., TPP. Data are reported as mean ± s.d., $n = 4$ gels analyzed for each experimental condition. Statistics: ***, $P < 0.001$; n.s., not significant (Student's t-test). d) AlamarBlue assay: total fluorescence generated by adherent NIH-3T3 cells. Data are reported as mean ± s.d., $n = 5$ gels analyzed. Statistics: **, $P < 0.01$ (Student's t-test). e,f) Total cell number/substrate area and cell spread area. Data are reported as mean ± s.d., $n = 3$ gels analyzed in triplicate for e) while $n = 50$ cells analyzed for each condition in (f). Statistics: ***, $P < 0.001$ (Student's t-test). g,h) Representative images of NIH-3T3 atop substrates at different chemical composition. i–k) Shear modulus, critical elongation and stress relaxation for substrates at identical chemical composition, i.e., $F_A = 0.14$, but different cross-linker, i.e., TPP or PPi. Data are reported as mean ± s.d., n = 3–4 gels analyzed for each experimental condition. Statistics: **, $P < 0.01$; n.s., not significant (Student's t-test). l) AlamarBlue assay for NIH-3T3 cells. Data are reported as mean ± s.d., $n = 5$ gels analyzed. Statistics: n.s., not significant (Student's t-test). m,n) Total cell number/substrate area and cell spread area. Data are reported as mean ± s.d., $n = 4$ gels analyzed in triplicate for m) while $n = 50$ cells analyzed for each condition in (n). Statistics: ***, $P < 0.001$; n.s., not significant (Student's t-test). o,p) Representative images of NIH-3T3 atop substrates at identical chemical composition but different cross-linker. Scale bar is 10 μm in (g), (h), (o), (p). All chitosan gels for this set of experiments were fabricated with molar ratio between the cross-linker and the repeating unit of chitosan, r = [TPP or PPi]/[chitosan]$_{r.u.}$, equal to 3.8.

partial conclusion for this analysis, it can be inferred that the higher the substrate dissipation energy the lower cell adhesion and spreading (Figure 4c).

We then attempted to identify the sugar sequences, i.e., the "dampers", responsible for such a behavior. We synthesized a library of chitosans encompassing F_A from 0.1 to 0.5 and plotted overall critical elongation of resulting gels as a function of polymer chemical composition (Figure 4d). A non-monotonic trend of γ_c was detected upon increasing chitosan acetylation, with an abrupt increment of critical elongation noticed around $F_A = 0.37$ followed by an almost matching drop. The non-monotonic trend is traced back to the presence of specific junctions, which act as energy dampers, likewise alternating MG sequences in alginates.[33] A mathematical modeling (Appendix 3, Supporting Information)[22] allowed determining the energy dampers which, irrespective of sugar position, embraced the following cases: the association of two 5-consecutive monomers (pentads) containing 1 and 3 *N*-acetyl-glucosamine units (A-type sugar), respectively, or two pentads containing 2 A-type sugars (Figure 4e).

3. Discussion

Collectively, our results provide evidence that substrate dissipation energy has a considerable impact on cell adhesion and spreading. Most of actual knowledge about cell-to-substrate relationship has been developed investigating linear stress–strain regime, where traction forces exerted by cells linearly deform the material.[1,8] Beside stiffness, recent findings have undoubtedly proved that even viscous contributions are key regulators of cell behavior.[13,15,19] Of note, it should be recalled that permanent

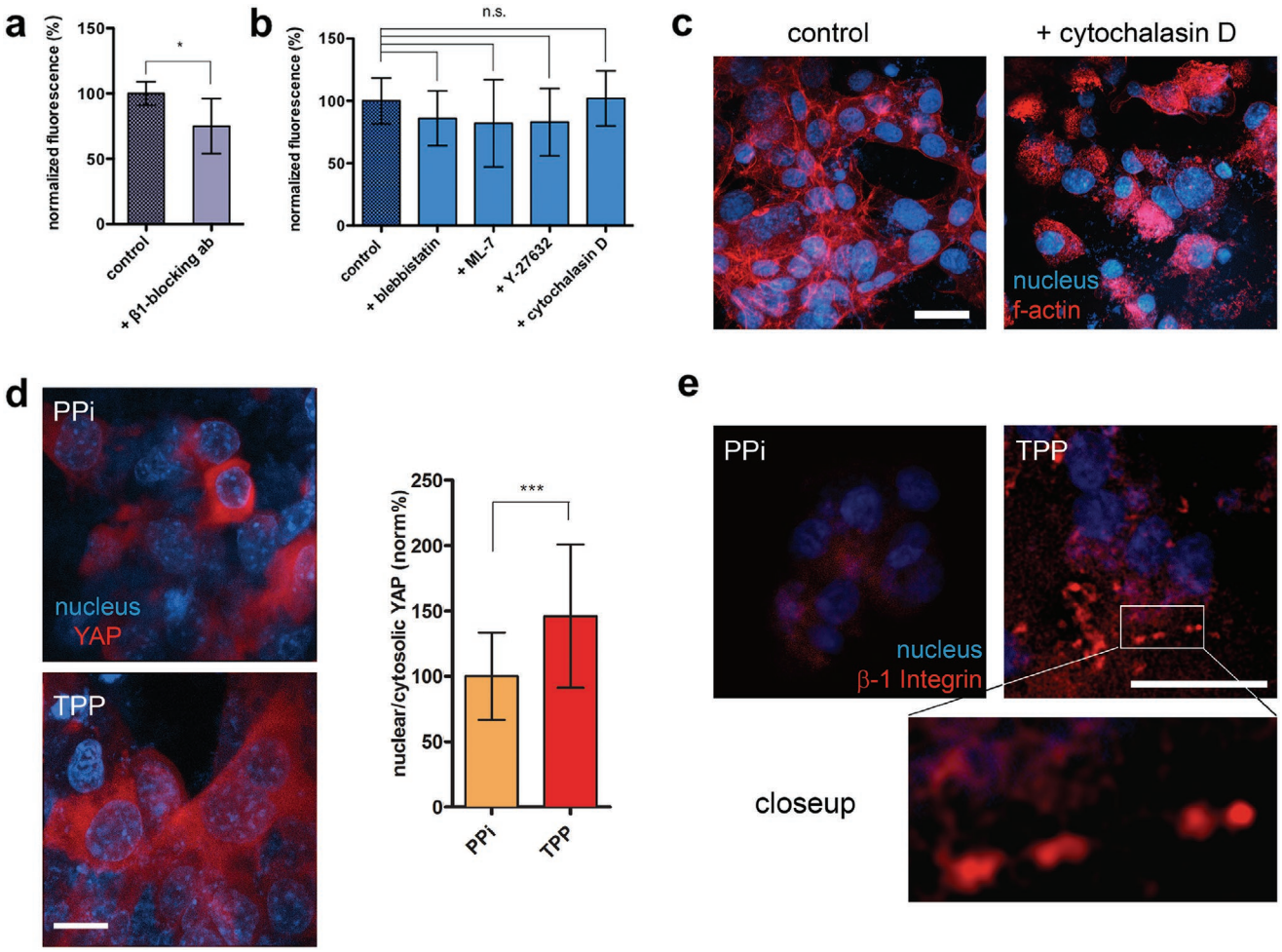

Figure 3. Cell adhesion and spreading atop chitosan-based substrates are temporally coordinated processes, the former mediated by β-1 integrin whereas the latter by cytoskeleton polymerization, YAP nuclear translocation and formation of punctual focal adhesions. a) Percentage of adherent MG-63 cells on $F_A = 0.14$ chitosan-TPP substrates in the presence or absence (control) of anti-human integrin β-1 monoclonal antibody. Total fluorescence generated by cells was normalized to that of control group, herein defined as 100% of adhesion. Data are reported as mean ± s.d., $n = 4$–5 gels analyzed. Statistics: *, $P < 0.05$ (Student's t-test). b) Percentage of adherent NIH-3T3 cells on $F_A = 0.14$ chitosan-TPP substrates in the presence or absence (control) of chemicals blebbistatin, ML-7, Y-27632, and cytochalasin D. Total fluorescence generated by cells was normalized to that of control group, herein defined as the 100% of adhesion. Data are reported as mean ± s.d., $n = 5$–8 gels analyzed. Statistics: n.s., not significant (One-way ANOVA followed by Dunnett's Multiple Comparison post hoc test). c) Representative images of NIH-3T3 on $F_A = 0.14$ chitosan-TPP substrates in the presence or not of actin polymerization inhibitor cytochalasin D. d) Immunostaining of YAP and nuclei together with quantification of YAP localization for NIH-3T3 cells on $F_A = 0.14$ chitosan-TPP and -PPi substrates. Data are reported as mean ± s.d., $n = 57$–58 cells analyzed for each condition. Statistics: ***, $P < 0.001$ (Student's t-test). e) Immunostaining of β-1 integrin-based punctual focal adhesions and nuclei for NIH-3T3 cells on $F_A = 0.14$ chitosan-TPP and -PPi substrates. Scale bar is 25 μm in (c), (d), (e).

and local ECM remodeling may occur due to plastic flow in the nonlinear region,[15,34] which depends in turn on the overall extent of linear stress–strain regime. Though often studied separately, it results of pivotal relevance underlining that these physical phenomena may occur simultaneously at ECM level, although at different time scales. Hence, the first objective of this work was to provide 2D substrates endowed with viscoelasticity but that may undergo mechanical plasticity (Figure 1).

Consistent with these premises, we hypothesized to systematically decouple substrate mechanics to correlate the dissipation of energy with cell response and, when taken together, our results reveal an interesting scenario. For low and medium dissipation energy substrates (F_A = 0.14 chitosan-TPP and -PPi gels, respectively), cells nicely adhered atop chitosan gels (Figure 2l,m). Stiffness moduli for this set of substrates resulted slightly higher (5.8 kPa, TPP case) and lower (2.8 kPa, PPi case) with respect to cell-ECM force transmission threshold required to trigger mechanotransduction processes.[29] Hence, substrate stiffness per se does not explain similar cell adhesion rate. On the other side, electrostatic contributions due to the cationic nature of chitosan can be safely ruled out, its residual net charge being equal to ≈10% at pH 7.4.[35] A further consideration stems from the comparable anchoring point distance and density of two systems. Since for PPi substrates the average network mesh size was 1.3-fold higher with respect to TPP counterparts (Appendix 2, Supporting Information), the relative mechanical feedback that cells gauged resulted only 2.2-fold lower ($W \propto \overline{\xi}^{-3}$),[9] therefore cells perceived similar loads

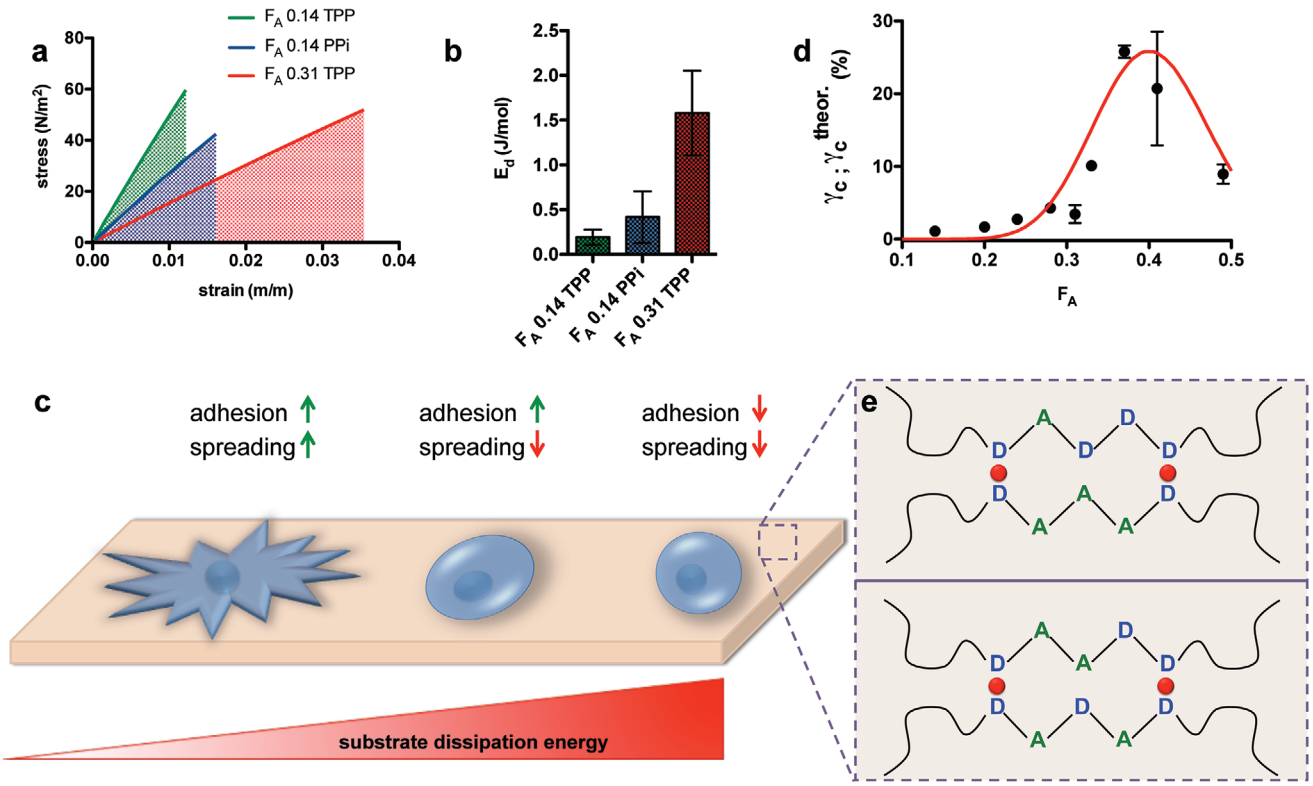

Figure 4. Cell adhesion and spreading are governed by substrate dissipation energy. a) Representative stress–strain curve profiles of chitosan substrates at different chemical composition ($F_A = 0.14$ or 0.31) and diverse cross-linker (TPP or PPi). Data are displayed up to the critical deformation at which substrate softening emerges. The dotted areas represent the energy at critical strain. b) Energy values are normalized for the crosslinking density, which is correlated to substrate stiffness. This approach allows identifying three different energy dissipation regimes, which can be related to cell adhesion and spreading behavior as c) depicted in the cartoon. d) Critical strain, γ_c, at which strain softening manifests for substrates at different chemical composition. Data for $F_A = 0.24$, 0.28, 0.33, 0.37, and 0.49 substrates have been replotted from our previous contribution,[26] and are reported as mean ± s.d. of at least $n = 3$ gels. The red solid line represents the best fitting of experimental points according to the mathematical model reported in Appendix 3 in the Supporting Information. e) For this set of substrates, we identified two possible combinations of five consecutive monomers (pentads) irrespective of sugar position: (i) the association of two pentads containing 1 and 3 *N*-acetyl-glucosamine units (A-type sugar), respectively; (ii) the association of two pentads containing 2 A-type sugars. These sugar sequences behave as "energy dampers," thus damping overall shear forces. Red spheres represent TPP as crosslink points between two close D-type (glucosamine) units.

as cue promoting cell adhesion. When the energy dissipation term was increased further as in the case of $F_A = 0.31$ chitosan-TPP gels (1.5 kPa as stiffness modulus), cell adhesion was vigorously hampered (Figure 2d,e). In this case the mechanical feedback was 4.1-fold lower, still very close to that produced by $F_A = 0.14$ chitosan-TPP substrates, thus insufficient to justify different cell behavior.[9] Rather than mechanical load, we therefore conclude that relative low substrate dissipation energy (≤0.42 J mol^{-1}) is essential in promoting adhesion growth. Our statement is strengthened by the fact that adhesion represents per se a physical event entailing dissipation of energy by cells.[36,37] Hence, it results clear that whole damping due to cell plus substrate contributions must be contained for permitting true cell adhesion.

When cell spreading is taken into account, additional considerations should be drawn. Our gels are viscoelastic, and intermediate viscosity was recently found to fully compensate reduced substrate stiffness in directing cell spreading, with optimal conditions uncovered for ECM stress relaxation falling in between clutching binding time (≈1 s) and its lifetime (up to 10^3 s).[19] Viscosity thus served to stiffen soft substrates; this "additional rigidity" abetted cell-ECM interactions and enhanced cell spreading through "load and fail" motor clutch system.[32] By comparing $F_A = 0.14$ chitosan-TPP gels versus -PPi counterparts, we detected different spreading rate (Figure 2n). Since both types of materials displayed stress relaxation in the order of 10^2 s (Figure 2k), we conjectured that viscosity-driven processes were out of determinants inducing different cell response. Here it should be recalled that our gels underwent irreversible plastic deformation (Figure S5, Supporting Information). The logical explanation resides therefore in the diverse material linear elongation, which associates with work generated by cells prior network yielding.[15] In the case of $F_A = 0.14$ chitosan-TPP gels, cells would exert traction forces adequate to overcome internal (due to viscous contribution, creep or work against actin polymerization)[20] and external (due to substrate) dissipation of energy, thereby entering into the plastic region where chitosan mesh can be remodeled likewise collagen or alginate-based IPN networks.[34,38] It results that cell spreading is energy-favored,[32] mediated by focal adhesion proteins clustering and YAP nuclear translocation (Figure 3d,e). If substrate dissipation energy is increased as for

F_A = 0.14 chitosan-PPi gels, cell traction forces are not adequate to exit efficiently from linear stress–strain regime; this translates to lack of focal adhesion formation, limited YAP nuclear translocation and, consequently, reduced spreading.

Our model (Appendix 3, Supporting Information) predicted that certain combinations of facing 5-consecutive monomers (pentads) damped shear forces, thus extending linear stress–strain regime. Since all chitosans used to build our substrates are in $^4C_1$ chair conformation resulting in diequatorial glycosidic linkages, the space between the first and every second sugar on same side of polymer chain is ≈1.04 nm.[39] Hence, the distance between the first and fifth monomer is estimated at 2.1 nm. We conclude that, upon adhesion, spreading decision was dictated by the effective work that cells generated in engaging transient molecular clutches with ensuing reduction of rearward movement of actin network without dissipation through 2.1 nm dampers.

4. Conclusions

In summary, our findings have proved original hypothesis about energy dissipation in determining cell behavior atop viscoelastic substrates.[15] Here we have determined three regimes of energy dissipation and correlated with cell-fate decisions: if the energy dissipation is low (0.19 ± 0.09 J mol^{-1}), cells can effectively earmark generated work in adhering and spreading. By progressively increasing substrate dissipation energy, cells lose the ability to spread (0.42 ± 0.29 J mol^{-1}) and adhere (1.58 ± 0.47 J mol^{-1}). Our results explain how low dissipation energy chitosan-based gels represent natural permissive substrates for cell adhesion without the need of grafted macromolecules as well as fibronectin, collagen, or any peptide sequences like RGD domains,[21] whilst RGD-free alginate-based materials, for instance, are not. Curiously, by adopting the approach reported in this work, we estimated the dissipation energy term of the alginate-Ca^{+2} gel system at 7.5 J mol^{-1} (Table S4, Supporting Information), thus falling into low adhesion and no spreading regime. Overall, here we report an experimental design that considers nonlinear strain-softening behavior as model of ECM mechanical plasticity. However, it should be mentioned that native ECMs could manifest also strain-stiffening effects,[40] hence additional work will be necessary in next future to understand whether cells would respond atop substrates at different dissipation energy showing nonlinear hardening.

5. Experimental Section

Chitosans Preparation and Characterization: Novamatrix/FMC Biopolymer (Sandvika, Norway) kindly provided the chitosan template (F_A 0.14) in base-form ($GlcNH_2$) used in this study.

To convert chitosan template into its chloride salt ($GlcNH_2$·HCl), the polysaccharide was solubilized under mild stirring using acetic acid 0.5% v/v (AcOH, Carlo Erba – Italy) as solvent at a final concentration of 0.4% w/v. Resulting chitosan solution was dialyzed as follows: NaCl 0.2 M (Sigma, USA), pH 4.5, 1 shift; deionized water, pH 4.5, 1 shift; deionized water, *n* shifts until the conductivity at T = 4 °C was below 3 μS cm^{-1}. The pH was adjusted to 4.5 using HCl 1 M (Carlo Erba, Italy) and finally the solution was freeze-dried.[26]

Chitosan template was reacetylated to a different extent following to the protocol reported elsewhere with slight modifications.[23] 1 g of chitosan template was solubilized at a final concentration of 1% w/v under mild stirring using AcOH 1% v/v as solvent. The final volume was 100 mL. Next, chitosan solution was diluted with an equal volume of ethanol (EtOH, Carlo Erba – Italy) and vigorously stirred. Finally, required amounts of acetic anhydride (Sigma, USA) were added, and solutions were stirred overnight. The molar ratio, *R*, between acetic anhydride and glucosamine unit of chitosan, i.e., R = [anhydride]/[$GlcNH_2$], was used as parameter to vary F_A (Table S1, Supporting Information). At the end of reaction, chitosan samples were converted into their chloride form as described above and freeze-dried.

The physical–chemical features of all chitosans were determined by viscometry, ^{1}H- and ^{13}C-NMR measurements. The intrinsic viscosity [η] of chitosans was measured at T = 25 °C by means of a CT 1150 Schott Geräte automatic measuring apparatus and a Schott capillary viscometer. A buffer solution composed by 20 × 10^{-3} M acetic acid/sodium acetate, AcOH/AcNa (Carlo Erba, Italy), pH 4.5, and 100 × 10^{-3} M NaCl was used as solvent.[26] Polymers were filtered through 0.45 μm Millipore cellulose filters (Merck, Germany) prior to the measurements. The F_A was determined by ^{1}H-NMR. Chitosan samples were prepared as follows: 20 mg of polymer were solubilized in 2 mL of D_2O + 150 μL of DCl (Sigma, USA) under vigorous stirring and mild heating. Then, 30 μL of sodium nitrite 10 mg mL^{-1} ($NaNO_2$, Sigma – USA) were added and the solutions stirred for 2 h.[26] Finally, 700 μL of chitosan samples were transferred into NMR tubes and analyzed at T = 80 °C by means of Varian MR-400 NMR spectrometer (9.4 T) equipped with a 5 mm X{^{1}H/^{19}F} ASW triple resonance broadband gradient probe. The fraction of dyads was determined by ^{13}C-NMR. 40 mg of polymer were solubilized in HCl 70 × 10^{-3} M and 20% v/v D_2O (final volume 2 mL). Then, $NaNO_2$ was added (40 mg $NaNO_2$/g chitosan), and solutions stirred for 4 h. Finally, the pH was raised up to 5 with NaOH 5 M and solutions transferred into NMR tubes. The ^{13}C-NMR measurements were carried out on a 500 VNMRS Varian NMR spectrometer (11.34 T) operating at 125.63 MHz for carbon, equipped with a 5 mm indirect detection broadband gradient probe. The spectra were recorded at T = 80 °C. 54000 scans were accumulated, using a spectral width of 31.250 kHz over 32 K complex point, with a recycle time of 1.4 s and a pulse width of 52°. The data were multiplied by a decaying exponential, with broadening factor of 3 Hz, and zero filled prior to FT. The dyad distributions were obtained from the integral ratios of Lorentzian lineshapes fitted to the experimental signals of C-6 by means of the Solver routine of Microsoft Excel. The physical–chemical characteristics of chitosan samples are summarized in Table S3 in the Supporting Information.

Substrate Preparation: Wall-to-wall cylindrical gels were fabricated by the slow ion diffusion technique with some modifications.[25] 66 mg of hydrochloride chitosans, together with 2.2 g of deionized water (3% w/v final concentration), were weighed into 5 mL beaker and stirred until complete polymer solubilization. Chitosan solutions were stored at 4 °C overnight and next casted into a mold (diameter = 22 mm, thickness = 2.5 mm) closed by two dialysis membranes (average flat width 33 mm cut-off 14000, Sigma – USA) and fixed by double circular stainless iron rings. The system was hermetically sealed and immersed into a gelling solution of Tripolyphosphate, TPP, or Pyrophosphate, PPi (Sigma – USA). The concentration of TPP and PPi in the gelling solution was varied based on chemical composition (F_A) of each chitosan, thus the molar ratio (*r*) between the cross-linker and repeating unit of chitosan (r = [TPP]/[chitosan]$_{r.u.}$) was set to 5.2 or 3.8 at the beginning of the dialysis.[28] The pH of TPP- or PPi-containing gelling solutions was adjusted to 4.50 ± 0.02 using HCl 5 M. Ion diffusion proceeded for 24 h under moderate stirring at room temperature allowing for gel formation.

Mechanical Characterization: Rheological characterization of chitosan gels was performed by means of a controlled stress rheometer HAAKE MARS III operating at T = 25 °C using a shagreened plate-plate apparatus ("HPP20 *profiliert*": diameter = 20 mm) as the measuring device. To avoid water evaporation from the gel, measurements were performed in a water-saturated environment formed by using a glass bell (solvent trap) containing a wet cloth. In addition, to prevent both

wall-slippage and excessive gel squeezing, the gap between plates was adjusted by executing a series of short stress sweep tests (ν = 1 Hz; stress range 1–5 Pa) until a constant G' was reached. The linear viscoelastic range was determined by means of stress sweep tests consisting in measuring elastic (G') and viscous (G'') moduli variation while increasing shear stress (1 Pa < τ < 1000 Pa) at a frequency ν = 1 Hz (hence with $\omega = 2\pi\nu = 6.28$ rad s^{-1}). The mechanical spectra (frequency sweep tests) were recorded by measuring the dependence of the elastic (G') and viscous (G'') moduli on pulsation ω at constant shear stress τ = 5 Pa (well within the linear viscoelastic range). Stress-relaxation tests have been conducted in steady state conditions using the following experimental conditions: strain, γ, 1% and time 600 s. Quantification of substrate plasticity was determined by creep-recovery measurements with τ = 100 Pa for 1800 s followed by τ = 0 Pa for 1800 s. The degree of plasticity was calculated as previously described.[34]

Swelling and Degradation Experiments: The structural stability of gels was verified in homemade prepared Hank's balanced salt solution (HBSS).[21] At the end of dialysis, TPP- or PPi-chitosan gels were laid down on filter papers to blot the excess of gelling solution. Gels were subsequently punched into small cylinders (diameter = 8 mm, thickness = 2.5 mm) by means of a disposable biopsy punch (Kai Medical, Japan), weighed by means of an analytical balance (time zero) and immersed in HBSS (V_{HBSS}/V_{gel} = 11, final volume = 1.38 mL). Samples were then placed at 37 °C under mild shaking. At selected time points, samples were removed from incubation medium, properly blotted and weighed. Finally, gels were placed again in fresh HBSS (which is replaced at each time point). Data are reported as % of mass gained/lost with respect to the initial weight, calculated as $[(W_t/W_0) - 1] \times 100$, where W_0 is the weight of gel at time zero, whereas W_t is the weight of the same gel at selected time.

Cell Culture: Mouse fibroblast-like NIH-3T3 (ATCC CRL-1658) and human osteosarcoma MG-63 (ATCC CRL-1427) were cultured in Dulbecco's Modified Eagle's Medium High glucose with 0.584 g L^{-1} L-glutamine and 0.11 g L^{-1} sodium pyruvate (EuroClone, Italy), supplemented with 10% heat-inactivated fetal bovine serum (Sigma, USA) and 1% penicillin/streptomycin (EuroClone, Italy), in a humidified atmosphere of 5% CO_2 at T = 37 °C.

Plating of Cells atop 2D Substrates: Chitosan as well as TPP- and PPi-based gelling solutions were prepared in sterile conditions and furthermore supplemented with 1% penicillin/streptomycin prior gelation. At the end of dialysis, TPP- and PPi-chitosan gels were washed by sterile deionized water in order to eliminate all residual traces of unbound cross-linker and next incubated in 20 mL of sterile phosphate buffered saline (PBS) (V_{PBS}/V_{gel} = 21) for 4 h at room temperature and mild shaking. Macroscopic gels were subsequently punched in sterilized conditions into small cylinders (diameter = 8 mm, thickness = 2.5 mm) by means of a disposable biopsy punch and further conditioned in fresh 20 mL PBS buffer at T = 37 °C for 1 h.[21] At the end of incubation, chitosan gels were laid down on 24-well plates and immediately covered with 1.8 mL of medium/well (V_{medium}/V_{gel} = 14.3) containing cells (250 000 cells per mL for the evaluation of cell adhesion, death, blocking adhesion and spreading inhibition experiments, whereas 80 000 cells per mL for immunostaining tests). Cells were incubated overnight in a humidified atmosphere of 5% CO_2 at T = 37 °C.

Evaluation of Cell Adhesion and Death: After overnight incubation, chitosan gels were moved in clean 96-well plates, washed extensively with PBS in order to remove nonadherent cells and incubated with 200 µL per well of AlamarBlue reagent (Sigma, USA), 10% v/v in complete DMEM medium for 4 h at T = 37 °C. At the end of this time frame, 150 µL of incubation medium were transferred into a black 96-well plate and the fluorescence was measured using a FLUOStar Omega-BMG Labtech spectrofluorometer (λ_{ex} = 544 nm; λ_{em} = 590 nm). The blank signal was measured from incubation medium of empty gels. The extent of cell death was evaluated by LDH assay (Sigma, USA). After overnight incubation, cell culture media were collected and the assay carried out as previously described.[21] The absorbance of samples was measured using a TECAN Microplate Reader at wavelengths of 490 and 690 nm.

Cell Immunostaining and Image Analysis: After overnight incubation, chitosan gels were moved in clean wells and washed extensively with PBS. Adherent cells were fixed with formaldehyde 4% v/v (Sigma, USA) in PBS for 30 min at room temperature. Then, gels were washed 5× with PBS and permeabilized with triton 0.2% v/v (Sigma, USA) in PBS for 15 min at room temperature. Next, gels were washed with PBS and incubated with BSA 4% w/v (Sigma, USA) + Normal Goat Serum 5% v/v (Sigma, USA) in PBS for 1 h at T = 37 °C. The blocking solution was then removed and the samples washed with PBS. The following primary antibodies were used for immunostaining: YAP antibody (dilution 1:200 or 0.5 µg mL^{-1}, sc-101199, Santa Cruz), Integrin β-1 antibody (dilution 1:500 or 0.4 µg mL^{-1}, sc-9970, Santa Cruz). Primary antibodies were diluted in blocking mixture. In the case of YAP, triton 0.1% v/v was also added to blocking mixture. Incubation proceeded overnight at 4 °C. Then, cells were washed and incubated with secondary antibody Mouse IgGk light chain diluted in blocking solution (dilution 1:300 or 1.3 µg mL^{-1}, sc-516179, Santa Cruz) for 2 h at room temperature. For the visualization of F-actin filaments and nuclei, cells were counterstained with Phalloidin-iFluor 594 Reagent (ab176757, Abcam, dilution 1:1000 in PBS) and DAPI 0.2 µg mL^{-1} (Sigma), respectively. Finally, chitosan gels were washed once and stored in PBS. Images from immunofluorescence and cellular staining experiments were acquired using a Nikon C1si confocal microscope (Nikon, Tokyo, Japan), equipped with 488 nm (argon), 408 nm, and 561 nm (diode) lasers. Light was delivered to the sample with an 80/20 reflector. The system was operated with a pinhole size of one Airy disk. Electronic zoom was kept at minimum values for measurements to reduce potential bleaching. For the different fields collected we used 40× and 60× Plan Apo objectives, saving series of optical images respectively at 200 µm x 200 µm or 100 µm x 100 µm with 2 µm z-resolution step size. Images in various conditions were captured under identical acquisition settings in order to allow comparison of fluorescent intensity, and were processed for maximum z-projection by using Fiji-ImageJ 1.52p (NIH, Bethesda, USA). The staining quantification was performed and analyzed by the ImageJ tool ROI manager. The degree of YAP nuclear localization was assessed as previously described.[29]

Blocking Adhesion and Spreading Inhibition Experiments: At the end of incubation in PBS buffer, chitosan gels were laid down on 24-well plates and immediately covered with 1.8 mL of medium/well containing cells in the presence of following chemicals: (±)-blebbistatin (50 × 10^{-6} M, Santa Cruz Biotechnology), ML-7 hydrochloride (25 × 10^{-6} M, Santa Cruz Biotechnology), Y-27632 dihydrochloride (10 × 10^{-6} M, Santa Cruz Biotechnology), and cytochalasin D (2 × 10^{-6} M, Santa Cruz Biotechnology).[15] Furthermore, cells were incubated with mouse anti-human integrin β-1 monoclonal antibody (dilution 1:200 or 5 µg mL^{-1}, clone P5D2, MAB1959, Merck – Germany). Chitosan gels were incubated overnight in a humidified atmosphere of 5% CO_2 at T = 37 °C. The day after they were moved in clean 24-well plates, washed extensively with PBS and incubated with the AlamarBlue mixture to quantify the percentage of cell adhesion as described above.

Statistical Analysis: One-way ANOVA (analysis of variance) was performed followed by Dunnett's Multiple Comparison post hoc test to evaluate differences among different groups and the control. An unpaired two-tailed Student's t-test was performed to evaluate differences between two groups. Differences were considered significant for P values less than 0.05.

Supporting Information

Supporting Information is available from the Wiley Online Library or from the author.

Acknowledgements

This study was supported by the INTERREG V-A ITALIA-SLOVENIA 2014–2020 BANDO 1/2016 ASSE 1 – project BioApp 1472551605 – granted to I.D. This work was also funded by FFABR, MIUR-University

of Trieste granted to G.B. Confocal images reported in this article were generated in the Light Microscopy Imaging Center of the University of Trieste at the Department of Life Sciences, funded as detailed at www.units.it/confocal.

Conflict of Interest

The authors declare no conflict of interest.

Author Contributions

P.S. and I.D. conceived and designed the experiments. P.S., G.B., and F.A. performed the experiments. P.S., G.B., F.A., E.M., and I.D. analyzed the data. P.S. wrote the paper.

Keywords

cell adhesion and spreading, energy dissipation, extracellular matrix viscoelasticity and plasticity, mechanotransduction, mechanotransmission

Received: March 2, 2020
Revised: April 20, 2020
Published online:

[1] D. E. Discher, P. Janmey, Y. L. Wang, *Science* **2005**, *310*, 1139.
[2] J. Swift, I. L. Ivanovska, A. Buxboim, T. Harada, P. C. D. P. Dingal, J. Pinter, J. D. Pajerowski, K. R. Spinler, J. W. Shin, M. Tewari, F. Rehfeldt, D. W. Speicher, D. E. Discher, *Science* **2013**, *341*, 1240104.
[3] D. E. Discher, D. J. Mooney, P. W. Zandstra, *Science* **2009**, *324*, 1673.
[4] T. Mammoto, D. E. Ingber, *Development* **2010**, *137*, 1407.
[5] T. Panciera, L. Azzolin, M. Cordenonsi, S. Piccolo, *Nat. Rev. Mol. Cell Biol.* **2017**, *18*, 758.
[6] G. Brusatin, T. Panciera, A. Gandin, A. Citron, S. Piccolo, *Nat. Mater.* **2018**, *17*, 1063.
[7] B. D. Hoffman, C. Grashoff, M. A. Schwartz, *Nature* **2011**, *475*, 316.
[8] A. J. Engler, S. Sen, H. L. Sweeney, D. E. Discher, *Cell* **2006**, *126*, 677.
[9] B. Trappmann, J. E. Gautrot, J. T. Connelly, D. G. T. Strange, Y. Li, M. L. Oyen, M. A. Cohen Stuart, H. Boehm, B. Li, V. Vogel, J. P. Spatz, F. M. Watt, W. T. S. Huck, *Nat. Mater.* **2012**, *11*, 642.
[10] M. Guvendiren, J. A. Burdick, *Nat. Commun.* **2012**, *3*, 792.
[11] V. Panzetta, S. Fusco, P. A. Netti, *Proc. Natl. Acad. Sci. USA* **2019**, *116*, 22004.
[12] Z. Liu, L. Bilston, *Biorheology* **2000**, *37*, 191.
[13] A. R. Cameron, J. E. Frith, J. J. Cooper-White, *Biomaterials* **2011**, *32*, 5979.
[14] O. Chaudhuri, L. Gu, D. Klumpers, M. Darnell, S. A. Bencherif, J. C. Weaver, N. Huebsch, H. Lee, E. Lippens, G. N. Duda, D. J. Mooney, *Nat. Mater.* **2016**, *15*, 326.
[15] O. Chaudhuri, L. Gu, M. Darnell, D. Klumpers, S. A. Bencherif, J. C. Weaver, N. Huebsch, D. J. Mooney, *Nat. Commun.* **2015**, *6*, 6365.
[16] S. Tang, H. Ma, H.-C. Tu, H.-R. Wang, P.-C. Lin, K. S. Anseth, *Adv. Sci.* **2018**, *5*, 1800638.
[17] M. Darnell, S. Young, L. Gu, N. Shah, E. Lippens, J. Weaver, G. Duda, D. Mooney, *Adv. Healthcare Mater.* **2017**, *6*, 1601185.
[18] J. Lou, R. Stowers, S. Nam, Y. Xia, O. Chaudhuri, *Biomaterials* **2018**, *154*, 213.
[19] Z. Gong, S. E. Szczesny, S. R. Caliari, E. E. Charrier, O. Chaudhuri, X. Cao, Y. Lin, R. L. Mauck, P. A. Janmey, J. A. Burdick, V. B. Shenoy, *Proc. Natl. Acad. Sci. USA* **2018**, *115*, E2686.
[20] J. Étienne, J. Fouchard, D. Mitrossilis, N. Bufi, P. Durand-Smet, A. Asnacios, *Proc. Natl. Acad. Sci. USA* **2015**, *112*, 2740.
[21] P. Sacco, F. Brun, I. Donati, D. Porrelli, S. Paoletti, G. Turco, *ACS Appl. Mater. Interfaces* **2018**, *10*, 10761.
[22] H. Grasdalen, B. Larsen, O. Smisrod, *Carbohydr. Res.* **1981**, *89*, 179.
[23] T. Freier, H. S. Koh, K. Kazazian, M. S. Shoichet, *Biomaterials* **2005**, *26*, 5872.
[24] K. M. Vårum, M. W. Anthonsen, H. Grasdalen, O. Smidsrød, *Carbohydr. Res.* **1991**, *217*, 19.
[25] P. Sacco, M. Borgogna, A. Travan, E. Marsich, S. Paoletti, F. Asaro, M. Grassi, I. Donati, *Biomacromolecules* **2014**, *15*, 3396.
[26] P. Sacco, M. Cok, F. Asaro, S. Paoletti, I. Donati, *Carbohydr. Polym.* **2018**, *196*, 405.
[27] H. Lee, L. Gu, D. J. Mooney, M. E. Levenston, O. Chaudhuri, *Nat. Mater.* **2017**, *16*, 1243.
[28] P. Sacco, S. Paoletti, M. Cok, F. Asaro, M. Abrami, M. Grassi, I. Donati, *Int. J. Biol. Macromol.* **2016**, *92*, 476.
[29] A. Elosegui-Artola, R. Oria, Y. Chen, A. Kosmalska, C. Pérez-González, N. Castro, C. Zhu, X. Trepat, P. Roca-Cusachs, *Nat. Cell Biol.* **2016**, *18*, 540.
[30] S. L. Gupton, C. M. Waterman-Storer, *Cell* **2006**, *125*, 1361.
[31] S. Dupont, L. Morsut, M. Aragona, E. Enzo, S. Giulitti, M. Cordenonsi, F. Zanconato, J. Le Digabel, M. Forcato, S. Bicciato, N. Elvassore, S. Piccolo, *Nature* **2011**, *474*, 179.
[32] C. E. Chan, D. J. Odde, *Science* **2008**, *322*, 1687.
[33] I. Donati, Y. A. Mørch, B. L. Strand, G. Skjåk-Bræk, S. Paoletti, *J. Phys. Chem. B* **2009**, *113*, 12916.
[34] S. Nam, J. Lee, D. G. Brownfield, O. Chaudhuri, *Biophys. J.* **2016**, *111*, 2296.
[35] P. Sorlier, A. Denuzière, C. Viton, A. Domard, *Biomacromolecules* **2001**, *2*, 765.
[36] E. Westas, L. M. Svanborg, P. Wallin, B. Bauer, M. B. Ericson, A. Wennerberg, K. Mustafa, M. Andersson, *J. Biomed. Mater. Res., Part A* **2015**, *103*, 3139.
[37] N. Tymchenko, E. Nilebäck, M. V. Voinova, J. Gold, B. Kasemo, S. Svedhem, *Biointerphases* **2012**, *7*, 43.
[38] K. M. Wisdom, K. Adebowale, J. Chang, J. Y. Lee, S. Nam, R. Desai, N. S. Rossen, M. Rafat, R. B. West, L. Hodgson, O. Chaudhuri, *Nat. Commun.* **2018**, *9*, 4144.
[39] T. T. Khong, O. A. Aarstad, G. Skjåk-Bræk, K. I. Draget, K. M. Vårum, *Biomacromolecules* **2013**, *14*, 2765.
[40] C. Storm, J. J. Pastore, F. C. MacKintosh, T. C. Lubensky, P. A. Janmey, *Nature* **2005**, *435*, 191.